

## Relationship of cloud top to the tropopause and jet structure from CALIPSO data

L. L. Pan<sup>1</sup> and L. A. Munchak<sup>1</sup>

Received 8 December 2010; revised 16 March 2011; accepted 24 March 2011; published 16 June 2011.

[1] Cloud top and tropopause relationships are examined using cloud top observations from the Cloud-Aerosol Lidar Infrared Pathfinder Satellite Observations (CALIPSO) cloud data and National Centers for Environmental Prediction Global Forecast System (GFS) tropopause data. Statistical analyses of cloud top occurrence in tropopause and jet referenced relative altitude coordinates are performed on a global scale using 4 years (2006–2010) of CALIPSO 5 km resolution cloud layer data. The results show that the thermal tropopause appears to be a significant constraint for the cloud top. The zonal vertical distribution of cloud tops in tropopause-relative coordinates shows a maximum at the tropopause level for both the tropics ( $20^{\circ}\text{S}$ – $20^{\circ}\text{N}$ ) and midlatitudes ( $40^{\circ}$ – $60^{\circ}\text{S}$ ,  $40^{\circ}$ – $60^{\circ}\text{N}$ ) for all four seasons. Occurrence of cloud tops above the tropopause is examined and quantified. The results show that with the consideration of tropopause height uncertainty, the data do not provide sufficient evidence of significant presence of cloud tops above the tropopause in the midlatitudes. In the tropics, the significant occurrences of cloud top above the thermal tropopause are found in regions known for seasonal deep convection. In most cases, the occurrence is up to 24% in  $2^{\circ} \times 3^{\circ}$  latitude-longitude bins with isolated higher frequencies in the western Pacific during the northern hemispheric winter season. The vertical distributions show that these events are mostly up to 2.5 km above the lapse rate tropopause, which is comparable to the differences between the lapse rate and the cold point tropopause in regions of active convection. We speculate that this separation may be responsible for a significant fraction of the cloud tops that do occur above the lapse rate tropopause in our analyses. It is also important to note that our results are limited by the CALIPSO twice-daily sampling with local equator crossing times of 0130 and 1330. The data therefore do not provide a good representation of convection over land, which is known to have maxima in afternoon local times. The tropopause determination is a significant component of this type of studies, and errors in the tropopause height may lead to significantly different conclusions. Our analyses show that the tropopause product from the GFS model is in better agreement with radiosonde measurements. The Goddard Earth Observing System Model Version 5 tropopause product, given as the ancillary data in the CALIPSO data file, shows a much larger uncertainty, primarily because the tropopause is identified at the model grid levels.

**Citation:** Pan, L. L., and L. A. Munchak (2011), Relationship of cloud top to the tropopause and jet structure from CALIPSO data, *J. Geophys. Res.*, 116, D12201, doi:10.1029/2010JD015462.

### 1. Introduction

[2] The tropopause is a fundamental boundary of the atmosphere, separating the turbulent mixing dominated troposphere from the much more stable and stratified stratosphere. The thermal tropopause as determined from the temperature lapse rate [World Meteorological Organization (WMO), 1957] marks a level of discontinuity in the static

stability. It has been shown that the change in background dynamical characteristics at this boundary has a fundamental impact on the distribution of chemical species. The thermal tropopause, therefore, often marks the chemical discontinuity between the stratosphere and the troposphere [Bethan et al., 1996; Tuck et al., 1997; Pan et al., 2004, 2009].

[3] In this work, we examine the role of the tropopause and the jet streams in constraining the cloud distributions, and in serving as a significant boundary for the top of the cloud in particular. Cloud formation and maintenance in the tropopause region is an active area of research. On the one hand, we expect the cloud distribution to be controlled by

<sup>1</sup>National Center for Atmospheric Research, Boulder, Colorado, USA.

the thermal and dynamical background. On the other hand, the radiative effect of the clouds is known to have a significant role in the thermal and dynamical structure of the UTLS region. For example, *Rosenfield et al.* [1998] estimated the influence of cloud heating on the local tropopause temperature structure and showed the potential impact of the temperature increase on the amount of water vapor transport into the stratosphere. *Corti et al.* [2006] showed the significance of cloud radiative effect in the tropical upwelling and in the transition from the Hadley circulation to the Brewer-Dobson circulation. The details of how clouds, especially thin cirrus, impact the overall structure of the tropopause region is still under active investigation [*Hartmann et al.*, 2001; *Yang et al.*, 2010]. Given the importance of clouds and cloud top distributions in our climate system, a quantitative understanding of how clouds are related to the background thermal and dynamical structure is an essential element for quantifying the role of clouds in a changing climate.

[4] Tropopause level clouds are a frequently observed feature. In the tropics, cirrus clouds at the tropopause level have been reported from both in situ and satellite observations [e.g., *Heymsfield*, 1986; *Nee et al.*, 1998; *Dessler et al.*, 2006]. In the extratropics, the cloud field is often seen to correlate with the structure of the tropopause and fronts [e.g., *Noël and Haefelin*, 2007; *Posselt et al.*, 2008]. In general, this is expected since abrupt changes in temperature and humidity, as well as vertical motion associated with frontal lifting, often occur at these dynamical boundaries. It is desirable to characterize this relationship globally and statistically. Cloud-Aerosol Lidar and Infrared Pathfinder Satellite Observations (CALIPSO) data provide an unprecedented opportunity for such characterization.

[5] The CALIPSO satellite was launched on 28 April 2006 to join the A-train constellation. The main instrument aboard CALIPSO is a polarized, dual frequency lidar operating at 1064 and 532 nm [*Winker et al.*, 2007, 2010, and references therein], which creates vertically resolved profiles of clouds and aerosols. Figure 1 shows a cross section of 532 nm attenuated backscatter from level 1 CALIPSO data, which gives an example of cloud and the relationship with the tropopause and jet stream. In this case, the tops of clouds in the tropics are near 17 km altitude and are apparently associated with the tropical tropopause. There is a significant change of the cloud top near the jet streams, which is especially abrupt in the Northern Hemisphere (NH), that marks the transition from the tropics to the extratropics. The strong correlation of the cloud top and the global tropopause structure shown by this and many other cases offered by CALIPSO data motivates this study. The goal of this work is to quantify this behavior in detail statistically.

[6] CALIPSO data have been used to examine cloud distributions from several different perspectives. For example, CALIPSO data have been used to characterize global distribution of cirrus clouds [*Nazaryan et al.*, 2008], the relationship between tropical cirrus clouds and deep convective clouds [*Sassen et al.*, 2009; *Massie et al.*, 2010], and cloud radiative effects [*Haladay and Stephens*, 2009; *Yang et al.*, 2010]. Our work aims to complement these analyses to connect the cloud occurrences to the dynamical background in the region of the upper troposphere and lower stratosphere (UTLS).

[7] One of the related science issues is the role of overshooting convection, in the tropics, versus slow ascent pro-

cesses in controlling the UTLS moisture and stratospheric water vapor budget [e.g., *Newell and Gould-Stewart*, 1981; *Danielsen*, 1993; *Holton and Gettelman*, 2001; *Sherwood and Dessler*, 2001; *Jensen et al.*, 2007]. The distribution of clouds in relationship to the tropopause is a key element in quantifying the controlling mechanism of water vapor transport into the stratosphere. A recent study using CALIPSO data has shown that there are significant occurrences of cloud above the tropopause, especially in the extratropics, which may have a significant impact on the stratosphere water vapor budget [*Dessler*, 2009]. There is indeed clear evidence of overshooting convection based on in situ measurements [*Hanisco et al.*, 2007; *Corti et al.*, 2008; *Khaykin et al.*, 2009]. It is not clear, however, if the in situ observed events are statistically significant or are isolated rare occurrences. The main goal of this work is to quantify the occurrence of cloud tops above the tropopause statistically using CALIPSO data along with tropopause heights from Global Forecast System (GFS) data.

[8] The quantitative results of this analysis are significantly constrained by the quality of available tropopause analyses on the global scale. One of the motivations of this work is to take a closer look at the role of the tropopause determination in the result of this type of studies. For this reason, we present an analysis comparing tropopause pressure from model analyses with that from the radiosondes. The results provide a rationale for using the National Centers for Environmental Prediction (NCEP) GFS tropopause product. This choice may be a significant factor that contributes to the differences between the conclusions of this work and those of *Dessler's* [2009] work, in which the tropopause is taken from the Goddard Earth Observing System Model Version 5 (GEOS5) analyses based ancillary data provided in the CALIPSO cloud layer data files. The comparisons of the two tropopause products are presented to justify our choice and to characterize the differences this choice may contribute.

[9] The final issue we explore is the role of the cold point tropopause (CPT) versus the lapse rate tropopause (LRT) in the tropics. It is known that the two often differ with the CPT higher than the LRT [e.g., *Seidel et al.*, 2001]. We look into some examples of clouds above the LRT in relation to the CPT and LRT differences and present an alternative perspective for the cloud tops found to be above the thermal lapse rate tropopause in the tropics.

## 2. Data

### 2.1. CALIPSO Data

[10] The CALIPSO satellite is on a Sun-synchronous polar orbit, with 0130 and 1330 local equator crossing times, and a repeat cycle of 16 days [*Stephens et al.*, 2002]. The lidar can detect clouds with optical depths as low as 0.01, but cannot penetrate clouds with optical depths greater than 5 [*Winker et al.*, 2010]. The measurements have a 30 m vertical resolution between -0.5 and 8.2 km above sea level, a 60 m vertical resolution between 8.2 and 20.2 km ASL and a 180 m vertical resolution above 20.2 ASL. Cloud layers are identified from the level 1 data using the selective, iterative boundary locator algorithm, described by *Vaughan et al.* [2009]. The cloud layer product is available in 1/3, 1, and 5 km horizontal resolutions; increasing averaging

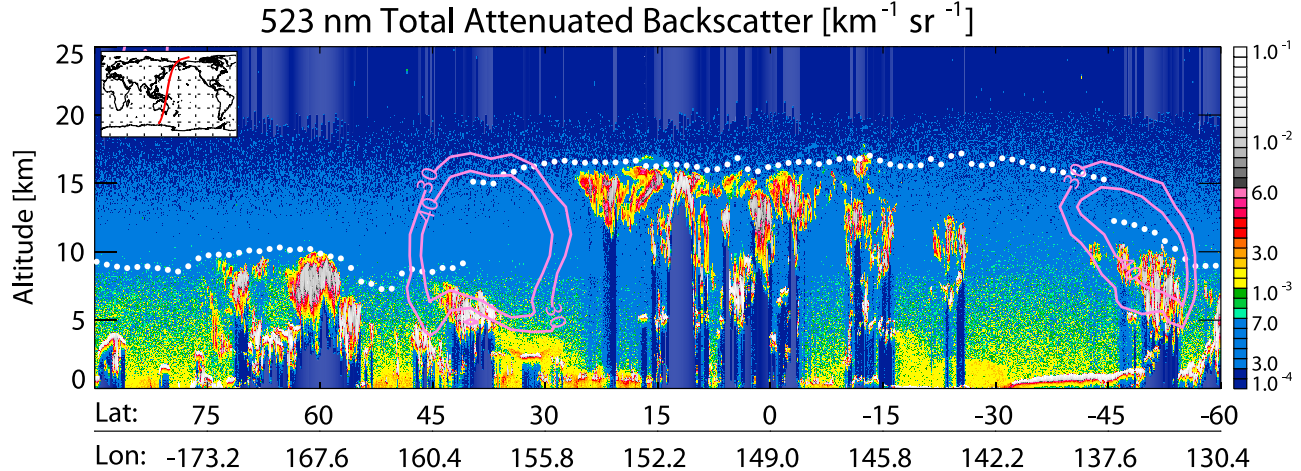


**Figure 1.** CALIPSO 532 nm lidar attenuated backscatter for a descending orbit on 13 March 2007 with equator crossing near 150°E and the meteorological background including the tropopause height (white dots) and jet stream locations based on wind speed (pink contours). The meteorological fields are from the GFS data.

increases the ability to detect weakly scattering features, including aerosols and thin cirrus. It is well known that the nighttime measurements (descending orbits) detect more cloud layers than the daytime measurements (ascending orbits) owing to higher sensitivity and a better signal-to-noise ratio [Nazaryan *et al.*, 2008; Liu and Zipser, 2009; Winker *et al.*, 2010]. This difference can result in 50–100% larger cloud fractions in night than in day [Dessler, 2009]. In this work, the version 3.01 5 km cloud layer (CLAY) product is used to identify the cloud top height (We have also analyzed version 2 data and found no significant difference between the two versions for the specific questions of interest to this work). This data product does not include clouds with both tops and bottoms above the tropopause. We have performed a sensitivity study to estimate the potential impact of misidentified clouds in aerosol layer data (ALAY), and the result is discussed in section 8. Four years of cloud layer data, both ascending and descending orbits, collected between June 2006 and May 2010, are used in our analyses.

## 2.2. OLR Data

[11] Outgoing longwave radiation (OLR) is commonly used as a proxy for deep convection. In this study, we use the  $2.5 \times 2.5$  degree interpolated daily mean OLR data available through the NOAA archive ([http://www.esrl.noaa.gov/psd/data/gridded/data.interp\\_OLR.html](http://www.esrl.noaa.gov/psd/data/gridded/data.interp_OLR.html)) [Liebmann and Smith, 1996]. The OLR in this data set is calculated from converting 10–12  $\mu\text{m}$  channel radiances measured by the Advanced High Resolution Radiometer (AVHRR) aboard the NOAA operational polar orbiting satellites. The daily mean is an average of one daytime and one nighttime measurement. The satellite used to estimate OLR during the time period of this study is NOAA 18, and has equator crossing times of 0155 and 1355 local, which is fairly similar to the CALIPSO equator crossing times.

## 2.3. GFS Data and the Tropopause

[12] The tropopause and other meteorological information used in this study is from the Global Forecast System (GFS) model, produced by the National Centers for Environmental,

Prediction (NCEP). The model truncation during this time period is T384L64. Two products are used in this study, the final analysis product (FNL), which is provided in  $1^\circ \times 1^\circ$  horizontal grids and 26 vertical levels (1000–10 hPa), and a high-resolution special product with  $\sim 0.3125^\circ \times 0.3125^\circ$  horizontal grids and 47 vertical pressure levels (1000–1 hPa). The FNL product is used for the statistical analyses while the high-resolution product is used for case studies. Both analyses are available four times daily. The GFS tropopause is calculated on the model's native 64 hybrid-sigma pressure level grid using an algorithm implementing the WMO thermal lapse rate tropopause definition [WMO, 1957] and interpolation between levels. Because the GFS tropopause is determined on its native grid, the tropopause heights given by the two products are nearly identical. The high-resolution tropopause has been found to be accurate to within 600 m when compared to radiosondes over the U.S. and NCAR/NSF Gulfstream V aircraft temperature measurements collected over the central United States during the Stratosphere-Troposphere Analysis of Regional Transport 2008 Experiment [Homeyer *et al.*, 2010; Pan *et al.*, 2010].

## 2.4. GEOS5 Data and the Tropopause

[13] The tropopause information given in the CALIPSO cloud layer data product is based on the Goddard Earth Observing System Model Version 5 (GEOS5) data with assimilated observations, developed in the NASA Global Modeling and Assimilation Office [Suarez *et al.*, 2008]. The model data are given in  $0.5 \times 0.666$  latitude by longitude grid by 72 Lagrangian control volume layers from the surface to 0.01 hPa. The tropopause information included in the CALIPSO data as part of ancillary data is from both version 5.1 (2006–2008) and version 5.2 (after 2008). The lapse rate tropopause pressure is determined using an algorithm based on the concept of skew-T diagram. For details, see the work of Rienecker [2008].

## 2.5. Radiosonde Data

[14] High-resolution radiosonde data are used in this work to evaluate the tropopause determination and the uncertainties

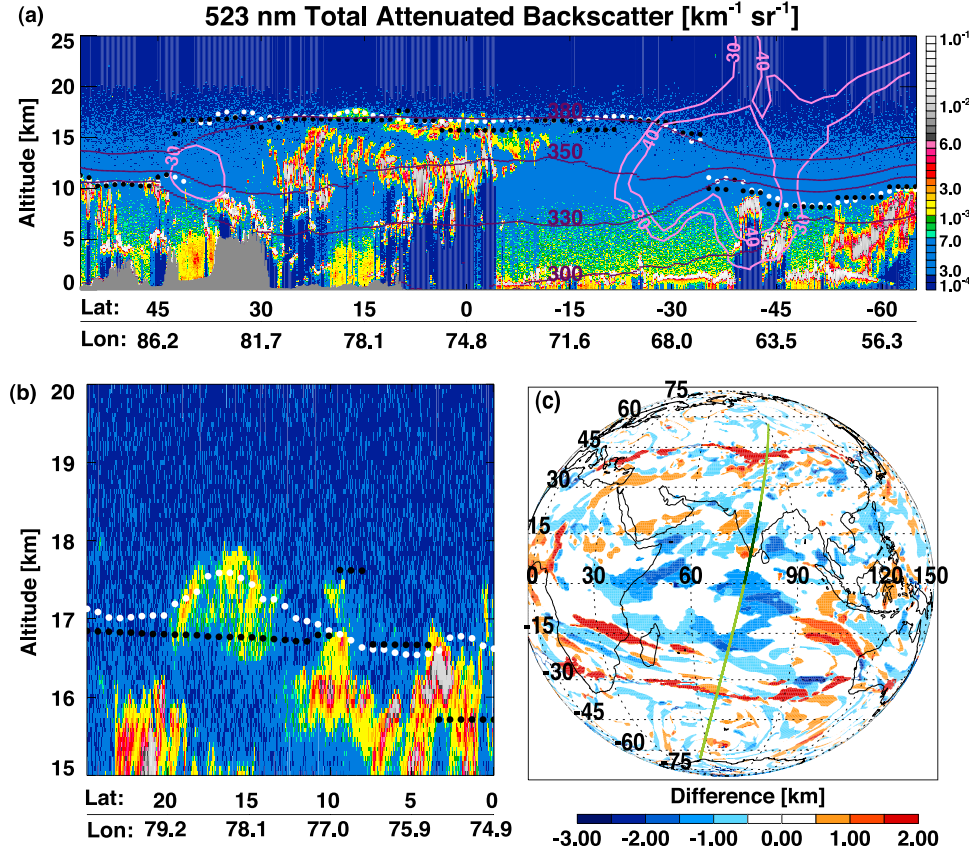


**Figure 2.** (a) CALIPSO 532 nm lidar attenuated backscatter for an overpass over Asia on 3 July 2007 beginning 2029:15 UT. Meteorology fields shown are wind fields (pink contours), selected potential temperature surfaces 300 K, 330 K, 350 K, and 380 K (purple lines), and the thermal tropopause height (white dots), from the high-resolution ( $0.5^{\circ}$  longitude  $\times 0.5^{\circ}$  latitude, 47 levels) GFS data interpolated to the CALIPSO orbit track. The black dots show the GEOS5 tropopause height given in the CALIPSO file. (b) Zoomed view for a segment of the track as indicated on the map. (c) Map of tropopause height differences between the two models (GEOS5-GFS) for 3 July 2007 at 1800 UT. The satellite overpass displayed in Figures 2a and 2b is shown in light and dark green, respectively.

of the tropopause products from GFS and GEOS5. The data are from the NOAA ESRL database. The tropopause level is part of the data product, derived from the temperature profile with approximately 40 m vertical resolution in the region of the tropopause. More than 70,000 profiles including midlatitudes and tropics from 3 months of JJA 2007 are used. More information about the data is available online: [http://www.esrl.noaa.gov/raobs/General\\_Information.html](http://www.esrl.noaa.gov/raobs/General_Information.html).

[15] In addition to above data, a special set of high vertical resolution ( $\sim 10$  m) radiosonde data is used in this work from the Tropical Chemistry, Cloud, and Climate Coupling (TC4) Ticosonde campaign in Costa Rica 2007. Around 200 sondes between July and August 2007, launched from Alajuela, Costa Rica [Pfister et al., 2010; Selkirk et al., 2010], are used to study thermal tropopause and cold point differences (section 7).

### 3. Issues of the Tropopause Determination and Uncertainty

[16] Since the goal of this work is to investigate the relationship between CALIPSO observed cloud top and the tropopause, errors and uncertainties in the tropopause deter-

mination are an important part of the analyses. In this section we discuss the issues of tropopause definitions and the impact of the uncertainty in the tropopause products.

[17] The conventional definition of the global tropopause is based on the temperature lapse rate and is termed as the thermal tropopause [WMO, 1957; Holton et al., 1995]. The thermal tropopause was designed to locate the critical change in the vertical gradient of the temperature and has been shown to mark the sharp increase in the static stability. In the tropics, a useful alternative to the lapse rate based thermal tropopause definition (LRT) is the cold point based thermal definition (CPT) [Selkirk, 1993; Highwood and Hoskins, 1998; Seidel et al., 2001]. In the extratropics, the alternative definition is the potential vorticity (PV) based dynamical tropopause, which was intended to mark the boundary on a given potential temperature surface, that is, the quasi-horizontal separation of stratosphere and troposphere [Hoskins, 1991; Holton et al., 1995; Kunz et al., 2011]. For the work of cloud top analyses, we consider the thermal tropopause as a more appropriate definition in the extratropics, since physically, the cloud formation is closely tied to the temperature and relative humidity. The thermal tropopause has been known to mark the critical

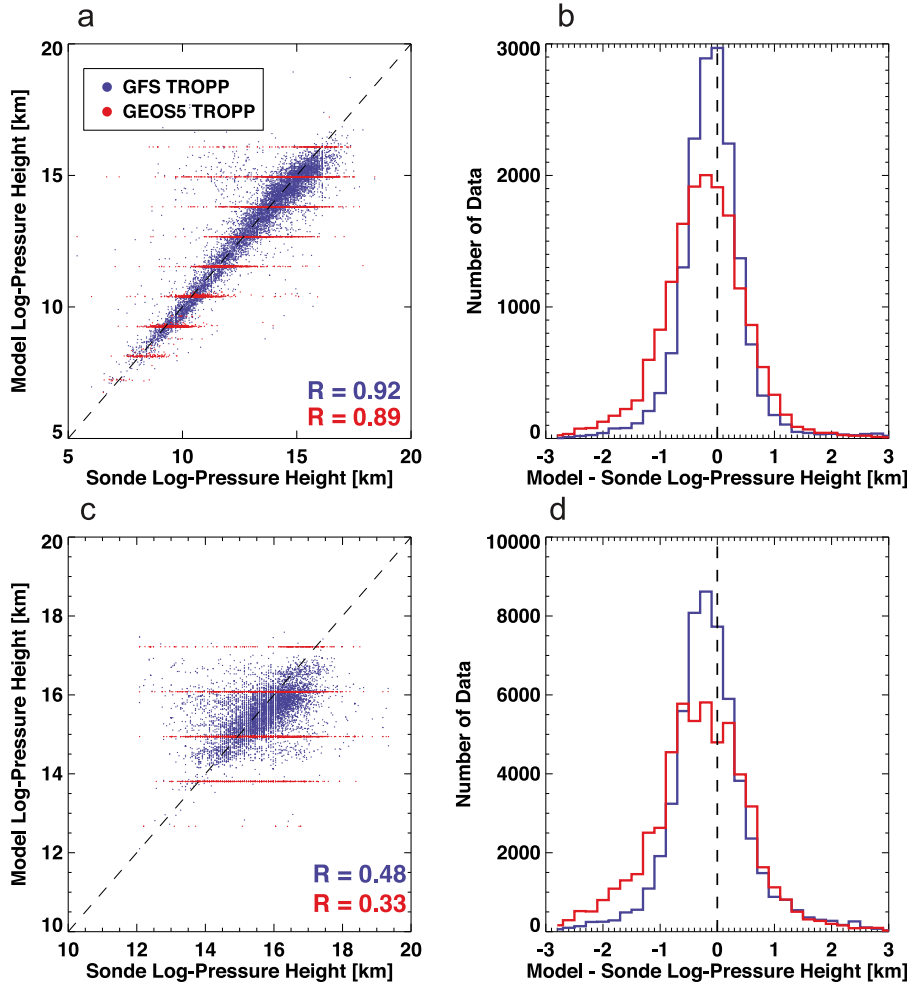


**Figure 3.** Comparisons of tropopause pressure (displayed in log pressure height) between the model analyses and the radiosonde measurements for the (a and b) midlatitudes and (c and d) tropics. The midlatitude sondes are all 0000 and 1200 UT sondes from the United States during June–August (JJA) 2007 (approximately 16,000 sondes). The tropical comparisons used 20°S–20°N data (approximately 56,000 sondes) during JJA 2007. The models are not interpolated but use the collocated time and the grid cell of the sonde launch. The GFS tropopause data are from the  $1^\circ \times 1^\circ$  latitude by longitude final analysis product. The histograms use a 200 m bin size. The GFS data are shown in blue, and the GEOS5 data are shown in red.

level of temperature gradient [e.g., Hoinka, 1997] and sharp relative humidity change [e.g., Pan *et al.*, 2000; Smith *et al.*, 2001]. We consider the cold point tropopause to be more relevant in the tropics for the same reason, but the global data we have do not provide the cold point. The possible limitations related to this issue are discussed in section 7.

[18] Before making the choice of using the GFS product, we have examined the tropopause data given in the CALIPSO level-2 data product, which is based on GEOS5 analyses. The results show that the GFS tropopause product is more accurate.

[19] Figure 2 shows an example of CALIPSO level-1 532 nm lidar backscatter and colocated GFS and GEOS5 tropopause heights. The cross section is from a nighttime, descending orbit. Two sets of colocated tropopause are shown. One from the GFS model and the other is taken from the CALIPSO data product and is based on GEOS5. The comparison shows that the GFS tropopause, in general,

better marks the background discontinuity indicated by the cloud layers. The discontinuous tropopause given by the GEOS5 product indicates that the tropopause height is given at the model grid levels, while the GFS tropopause is not limited to the grid levels.

[20] To evaluate these two products beyond isolated cases, we have made comparisons with a large set of radiosonde data. Figure 3 shows comparisons of two tropopause products from analyses with the radiosonde tropopause for JJA 2007 over two regions, the continental United States and the tropics (20°S–20°N). More than 70,000 profiles are used in these comparisons. It is evident from Figure 3 that the much larger uncertainty in the GEOS5 tropopause may be contributed foremost from the factor of locating the tropopause on the model grid levels. The higher accuracy of the GFS tropopause is shown by the sharply peaked probability distribution of GFS-radiosonde tropopause differences (Figures 3a and 3c). Statistically, in the case of GFS,

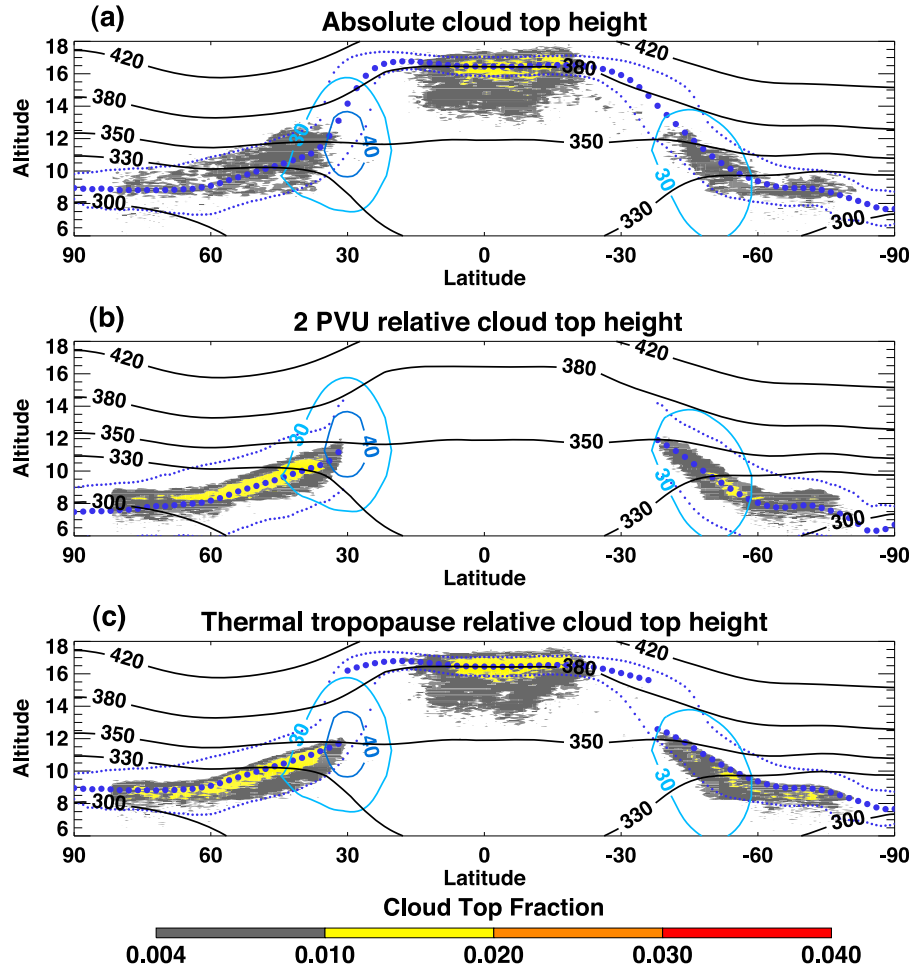


**Figure 4.** Vertical distribution of the cloud top fractions calculated in three different reference levels together with the dynamical background. (a) The cloud fraction (color shading), binned in  $1^{\circ}$  latitude for all longitudes ( $-180^{\circ}$ – $180^{\circ}$ ) horizontally and 60 m vertically (in CALIPSO native levels near the tropopause), in geometric altitudes. Also shown is the zonal mean tropopause height (large purple dots) and its tenth and ninetieth percentiles (small purple dots), zonal mean horizontal wind speed (blue contours for 30 and 40 m/s), and zonal mean potential temperature surfaces (black lines). (b) The cloud fraction vertically binned in altitude relative to the dynamical tropopause using 2 potential vorticity units (PVU) surface for the extratropics. The zonal mean dynamical tropopause (large purple dots) and its tenth and ninetieth percentiles (small purple dots) are shown. (c) The cloud top fraction in altitude bins relative to the thermal tropopause, with the zonal mean, tenth, and ninetieth percentiles same as above. The average is from 1 to 31 March 2007. Dynamical fields are from the GFS data. See text for more details about this calculation.

the result is consistent with the previous study by Homeyer *et al.* [2010] in that the GFS show a low bias of  $\sim 70$  m and the standard deviation of uncertainty is  $\sim 650$  m. In case of the GEOS5 product, there is a statistical low bias of  $\sim 140$  m and standard deviation of  $\sim 1$  km in the United States. These results support our choice of using the GFS tropopause product in the following cloud top analyses.

#### 4. Method of Analysis: Introducing the Tropopause Relative Coordinates

[21] The statistical relationship between the cloud top and the tropopause is analyzed by first calculating the level of the cloud top relative to the level of the colocated tropopause. The frequency of occurrence is then calculated in

selected vertical and horizontal bins. In this calculation, each profile in the 5 km cloud layer data is considered as a measurement. If there is cloud determined in the profile, the level of the cloud top for only the highest layer is considered. The frequency of occurrence is binned vertically in 60 m, which is the native resolution of the cloud layer data file. The tropopause height is from GFS data using the nearest data in space and time. Examples of frequency of occurrence using three different reference levels are shown in Figure 4 to motivate the use of a tropopause relative coordinate. In all three cases of Figure 4, the zonal averages are done for every 1 degree latitude band globally for March 2007.

[22] The thermal tropopause relative coordinates have been used extensively in chemical tracer analyses [e.g., Tuck *et al.*,

1997; *Pan et al.*, 2004, 2007; *Tilmes et al.*, 2010] and in temperature profile analyses [e.g., *Birner*, 2006]. In general, this coordinate is defined using the thermal tropopause height as the reference point; that is, the tropopause level is set to be zero. When displaying vertically, it is often more helpful to adjust the reference altitude to the mean tropopause height. The relative altitude,  $Z_r$ , in this coordinate is defined as

$$Z_r = \bar{Z}_{trop} + (Z - Z_{trop}), \quad (1)$$

where  $Z$  is the measurement altitude relative to the sea level,  $Z_{trop}$  is the colocated simultaneous tropopause height, and  $\bar{Z}_{trop}$  is the mean tropopause height for the range of the statistical calculation.

[23] To demonstrate the application of the tropopause relative coordinates, vertically binned cloud top occurrence frequency, using one month of data (March 2007), in three different coordinates together with the zonal mean dynamical background are shown in Figure 4. Figure 4a shows the distribution in regular altitude coordinates, that is, in sea level based altitude. In Figure 4b the cloud top is binned in relative altitudes to the 2 potential vorticity units (PVU) level for the extratropics only. Figure 4c shows the distribution using the thermal tropopause relative coordinates, as defined in equation (1). To indicate the range of variability in the tropopause height, we have also given the tenth and ninetieth percentile of the corresponding tropopause height in each case.

[24] The three cases shown in Figure 4 have some gross similarities, including the overall pattern of cloud top frequency clustered around the tropopause in both tropics and the extratropics. In detail, however, significant differences exist. In Figure 4a, using statistics in a sea level referenced altitude, the distribution shows significant cloud top fractions above the tropopause both in the tropics and the extratropics, especially in the northern midlatitudes. This behavior changes in Figure 4c, especially in the extratropics. When the statistics are done in tropopause relative coordinates, the cloud tops are maximized at or below the tropopause in the extratropics with a consideration of 0.65 km tropopause uncertainty in the GFS data. This point will be examined in detail in section 6.

[25] When tropopause relative altitudes are used, the cloud top distributions become much more compact. In the case of using the 2 PVU defined dynamical tropopause as the reference level (Figure 4b), we find the reference level (the dynamical tropopause) roughly marks the center of the band of the high cloud top occurrence (Note that the highest 2 PVU surface is used in case of multiple values). This is not a surprise since the 2 PVU level is known to be lower than the thermal tropopause statistically [e.g., *Hoerling et al.*, 1991], and it can be significantly lower (up to several kilometers) in cases of deep stratospheric intrusion events [e.g., *Shapiro*, 1980; *Pan et al.*, 2007, 2010] where frontal clouds are often above the 2 PVU level. Chemical tracer analyses also show that a dynamical tropopause determined by a fixed PV value do not mark well the discontinuity of the chemical tracer across the boundary of stratosphere and troposphere [*Pan et al.*, 2004]. The thermal tropopause, which marks the discontinuity of the temperature structure and a sharp change in relative humidity [e.g., *Pan et al.*, 2000; *Smith et al.*, 2001], is a better choice in cloud top studies.

[26] In addition to the PV based extratropical tropopause, we need to consider the cold point based tropical tropopause. The difficulty is that a faithful identification of the cold point requires high vertical resolution data that are not available in high-density global coverage [e.g., *Seidel et al.*, 2001]. The lack of the cold point tropopause information leads to potentially the most significant uncertainty in the conclusions of this study. Section 7 is dedicated to this problem.

[27] Note that the global zonal mean tropopause height in Figures 4a and 4c are different, highlighted by the presence of a significant tropopause break in Figure 4c. The zonal mean tropopause heights are calculated differently in these two examples to highlight the fact that the distribution of the tropopause height near the subtropical jet is known to have a bimodal structure. This structure has been shown in many prior studies for the Northern Hemisphere and is highlighted by the separation of the tropical and extratropical tropopause height near 14 km in altitude or 150 hPa in tropopause pressure [e.g., *Hoinka*, 1997; *Pan et al.*, 2004; *Seidel and Randel*, 2007]. Since the break follows the jet stream, which meanders in a range of latitudes, the zonal average usually produces a ~14 km mean tropopause height near the subtropical jet, as shown Figure 4a. Here we propose a more meaningful way of zonal averaging that represents the bimodal structure. This result is shown in Figure 4c, where the tropopause height is averaged, in each 1° latitude band, in two groups using 14 km as the separation level. The break represents the latitude band where more than 50% of the tropopause on one side is below 14 km and on the other side is above. This break has an excellent agreement with the zonal mean jet core position in the Northern Hemisphere. The tenth and ninetieth percentiles are shown for each latitude bin as an indication of variability and the range of overlap between the tropical and the extratropical tropopause.

## 5. Vertical Structure in the Asian Monsoon Sector

[28] Using the method described in section 4, we examine the seasonal behavior of the cloud top distribution relative to the tropopause for the Asian monsoon sector. We choose this region because the Asian summer monsoon system is known to be a significant pathway for troposphere to stratosphere transport in the NH summer [*Dethof et al.*, 1999; *Randel et al.*, 2010]. Enhanced UTLS water vapor signature over the Asian monsoon is found in previous studies [*Randel et al.*, 2001] and is attributed to the deep convection in the region. The cloud top distribution over the Bay of Bengal versus that over the Tibetan Plateau is also of special interest. Recent studies question which system, the convection over the Bay of Bengal or the Plateau, dominates the transport into the upper level anticyclone [*Fu et al.*, 2006; *James et al.*, 2008; *Park et al.*, 2009; *Devasthale and Fueglistaler*, 2010]. The CALIPSO cloud top frequency in relation to the mean tropopause height in this region has been examined for contribution to water vapor transport across the tropopause [*Dessler*, 2009]. In this section we examine the vertical structure of the region and whether there is an anomalous cloud top and tropopause relationship using GFS colocated thermal LRT height. A longitude sector, 70°–110°E, is selected which includes the Bay of Bengal and the Tibetan Plateau.

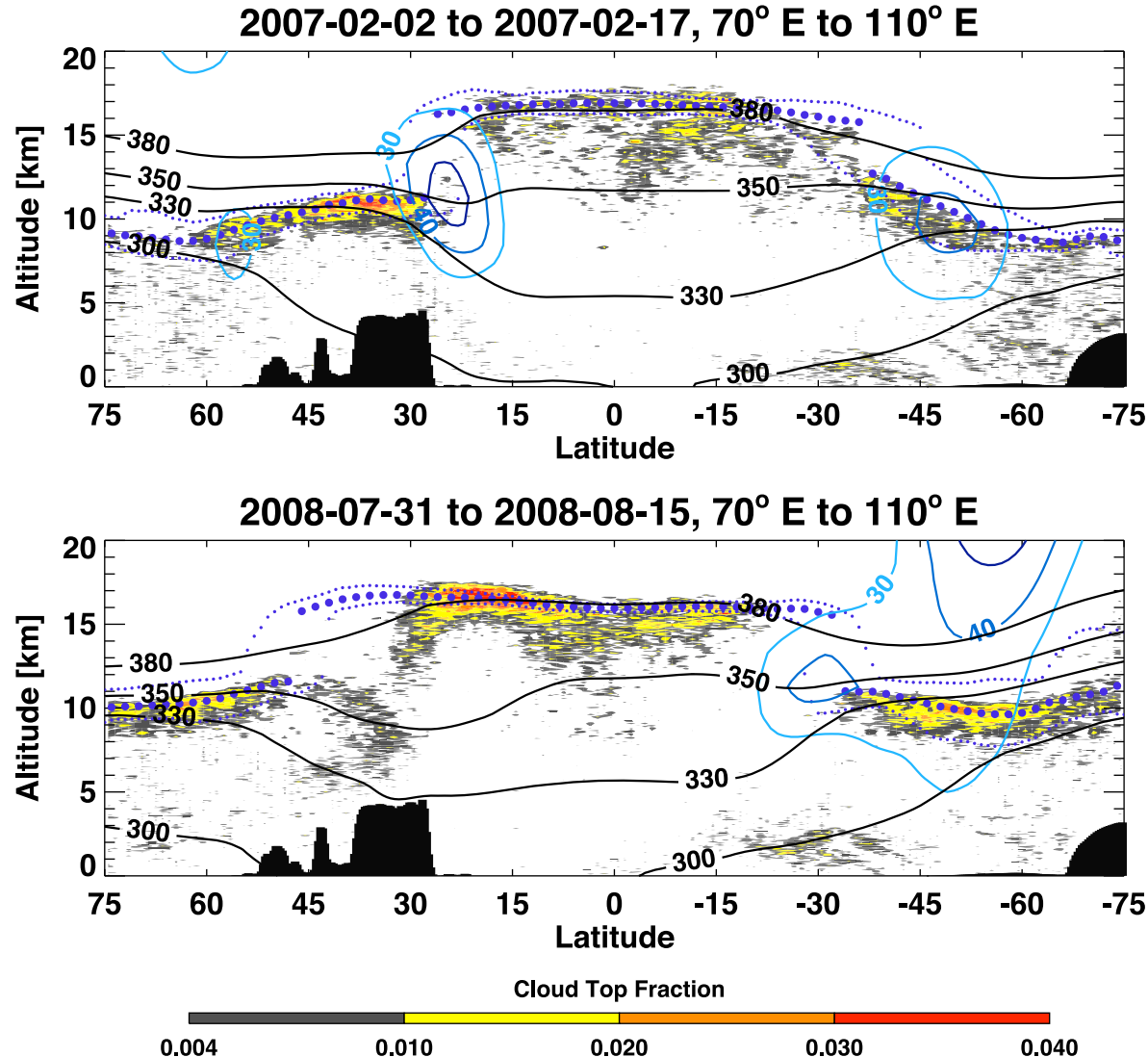


**Figure 5.** Fraction of cloud top for a sector over the Asian summer monsoon region (Bay of Bengal and the Tibetan Plateau, 70°–110°E) for two selected periods each including 16 days (CALIPSO orbit processing cycle). The tropopause, the wind, and the potential temperature fields are averaged over the same sector, represented in the same way as in Figure 4c. The topography at 86.5°E is also shown.

[29] The vertical structure of the cloud top is examined in two sets of statistics. The first set is near “instantaneous,” where the fraction is calculated using the minimum sampling time period of 16 days, in which the satellite orbit procession completes a cycle [Stephens *et al.*, 2002]. We examined the period of 2007–2008, and two selected frames are given in Figure 5 as examples. The second set of statistics is calculated using maximum sampling for seasonal fractions including all four years of data. The result for December–February (DJF) and June–August (JJA) seasons are shown in Figure 6. These two sets of analyses complement each other in showing variability and the statistical behavior of the vertical structure. In both cases, the vertical cross section is constructed as in Figure 4c, using the tropopause relative coordinate together with the zonal mean tropopause and wind field showing the jet locations. In each case, the tenth and ninetieth percentile tropopause height for

the ensemble relevant to the cloud sampling are given to indicate the background variability.

[30] Figure 5, contrasting February and August, shows a significant difference in the tropopause heights. The region of the Plateau, ~20–40°N, is poleward of the subtropical jet in February with an ~11 km mean tropopause height, but it is covered under the high tropical-like tropopause in August during the monsoon season. In fact, the tropopause height over the Plateau during this time is higher than that in the equatorial region (see section 5 and Figure 8 for details). The cloud top distributions for the two observation periods are also quite different, especially in the monsoon region. There is a significantly higher frequency of occurrence at and around the tropical tropopause in August, especially in the region over the Bay of Bengal (~10–20°N). In the region over the Plateau (~20–40°N), the cloud top distribution is spread out over a large range in the vertical, between 6 to

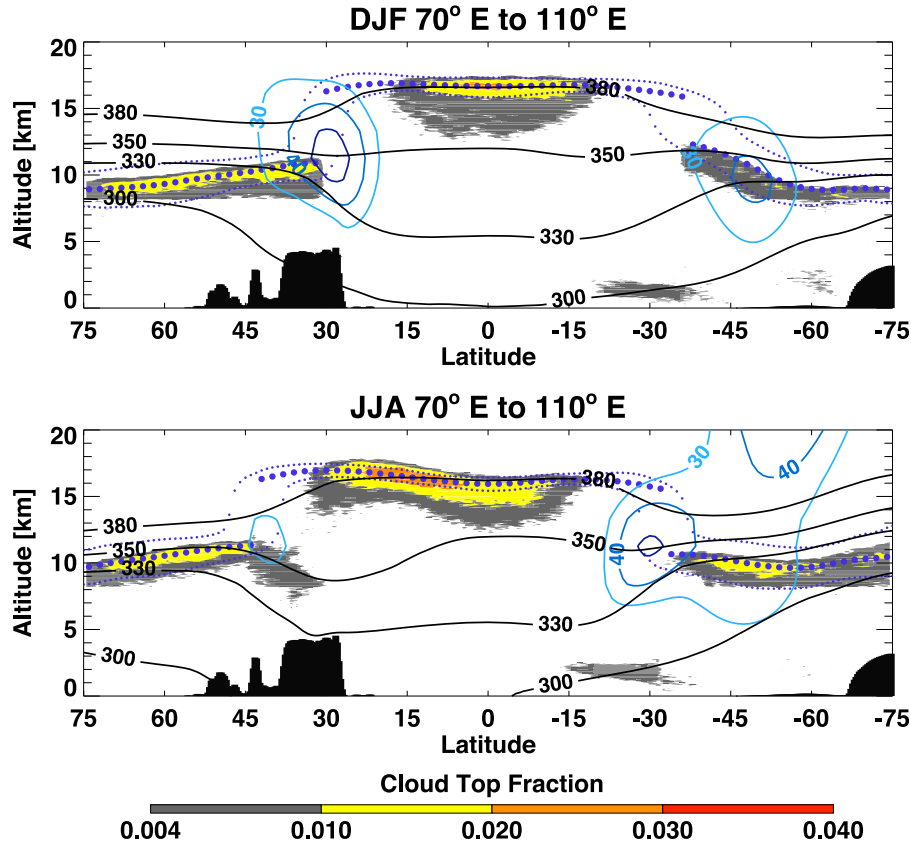


**Figure 6.** Vertical structure of seasonal cloud top fractions over the Asian monsoon sector ( $70^{\circ}$ – $110^{\circ}$ E) for December–February (DJF) and JJA seasons. Data include 4 years from 13 June 2006 to 31 May 2010. The tropopause, the horizontal wind, and the potential temperature fields are averaged over the same sector and represented in the same way as in Figure 4c. The topography at  $86.5^{\circ}$ E is also shown.

12 km over the northern edge and up to the tropical tropopause altitudes over the southern edge. These are clear indications of convection that is active during the summer monsoon season. The distribution also indicates that the convection from the Plateau results in cloud tops below the core of the Asian monsoon anticyclone ( $\sim$ 12–14 km) [e.g., Randel and Park, 2006]. This result, however, may be influenced by the limited sampling time, further discussed later in the section.

[31] In the extratropics, defined as the region with a tropopause height below 14 km, the February and August observations are similar to each other in showing the cloud top clustered at and below the tropopause to within the uncertainty of the tropopause height determination. The occurrence above the tropopause will be quantified in section 6, but here we note that this result is significantly different from the conclusions of Dessler [2009], in which the maximum cloud top fraction is found to be above the tropopause and a significant occurrence (0.1% or more) is found to be around 3 km or 40–50 K potential temperature above the tropopause. On the basis of our result, the significant overestimate of cloud top in the work of Dessler [2009] may be a result of a larger tropopause uncertainty and comparing the cloud statistics with the mean tropopause height instead of the colocated tropopause height. We note that this difference is similar to that shown by the examples in Figure 4.

[32] The seasonal statistics using all four years of data, as shown in Figure 6, is very similar to the near instantaneous vertical cross section shown in Figure 5. Together, Figures 5 and 6 show several characteristics of cloud top distributions during the monsoon season. Accompanying the high tropopause, the region of the Bay of Bengal has significant increases in high cloud tops compared to the NH winter season with cloud top frequently appearing to be above the model thermal tropopause. There are significant fractions of cloud tops vertically distributed between 7 to 17 km over the Tibetan Plateau, with the higher distributions over the southern side and the lower distributions over the northern side. The cloud tops do not show significant fractions above the tropopause in the extratropics. More quantitative analyses of these behaviors will be given in section 6.

[33] Although it is not the focus of this work to study low clouds, we note the layer of low cloud tops over 15–40 S in Figure 6 for both DJF and JJA seasons. This interesting climatological feature is found over the southern Indian Ocean, west of Australia. These persistent low clouds, over the subtropical marine boundary are observed in prior studies. In particular, Bony *et al.* [2000] have analyzed extensively the high frequency of occurrence of marine low cloud during January and February (>50%) in the region of the southern Indian Ocean. What makes this region stand out in our analyses is the lack of high clouds in this region, since we only count the highest cloud tops when there are multiple layers.

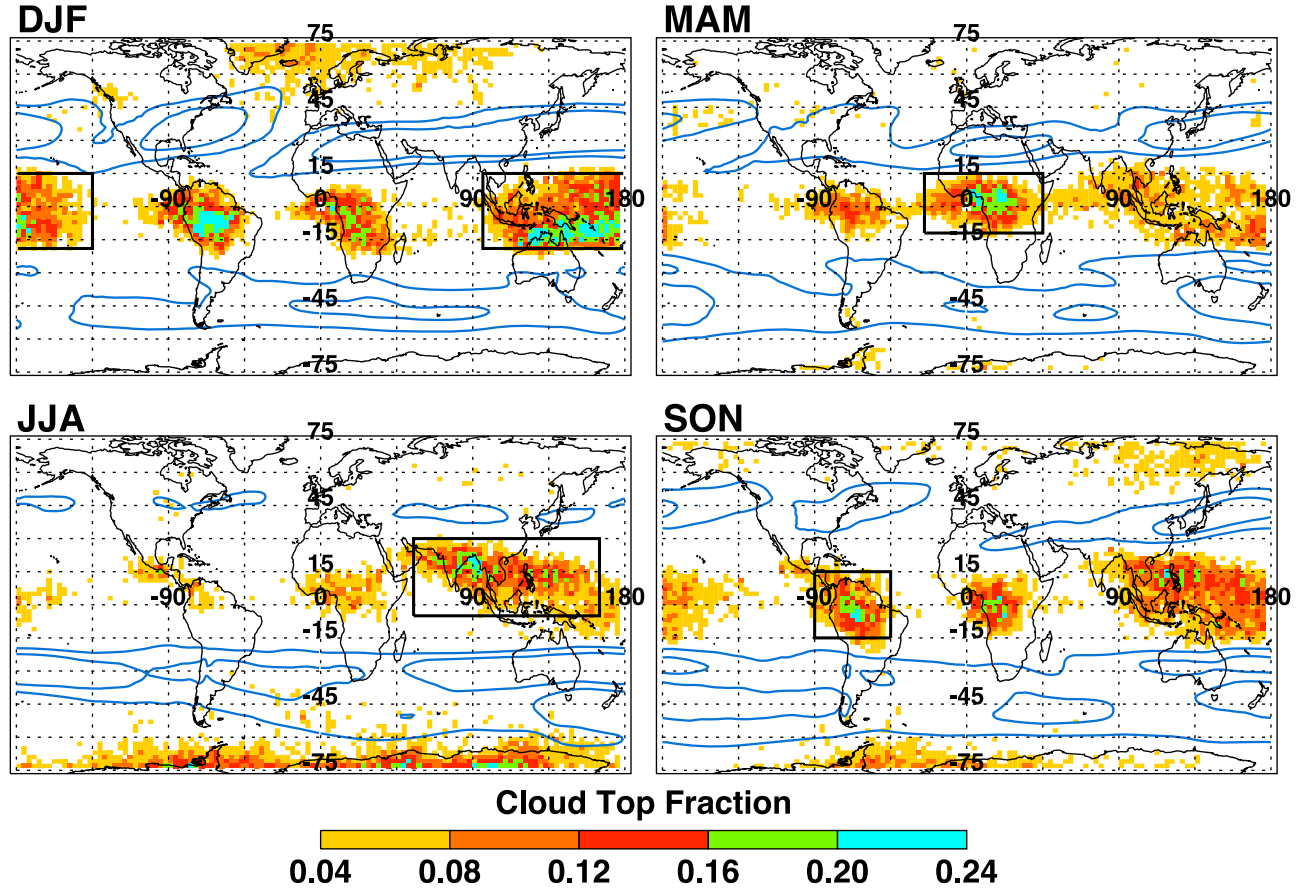


**Figure 7.** Maps of cloud top fraction above 0.5 km above the GFS thermal tropopause. Horizontal wind speed at 200 hPa is shown in blue contours (30 and 40 m/s). The cloud fractions are given in  $3^\circ \times 2^\circ$  longitude versus latitude bins. The calculation includes 4 years of CALIPSO data as in Figure 5. The rectangles indicate the selected regions of frequent overshooting cloud tops and will be examined in more detail in Figure 10.

[34] We note that the CALIPSO data based statistics suffer from the limitation of twice-daily sampling with a 0130 and 1330 local equator cross time. This limited sampling time will bias the observations toward the oceanic convection, since the convection events in the regions involved are known to have different diurnal cycles. In general the oceanic convection has a weak diurnal cycle and is more nocturnal with the maximum near midnight. The land convection has a strong diurnal cycle that reaches a maximum in the afternoon [e.g., Liu and Zipser, 2005; Liu *et al.*, 2008]. Because of this sampling issue, CALIPSO or A-train data in general are not suited for a conclusive study of the relative role of land versus ocean convection. When we interpret the statistics shown in Figures 5 and 6, it is important to keep this in mind.

## 6. Distribution of Cloud Tops Above the Tropopause

[35] The vertical distributions of cloud top shown in Figure 6 indicate that there are seasons and regions that have significant events of higher cloud tops than the model determined LRT. We examine these distributions in more detail in this section, both geographically and vertically.

[36] As indicated in Figures 5 and 6, the range of cloud top above the local tropopause is very similar to the variability of the tropopause, which is represented by the ninetieth percentile in Figures 5 and 6. The uncertainty in the tropopause determination is often of the same magnitude. Considering the limitation of the tropopause information, we choose a somewhat subjective criterion of 0.5 km (a comparable but less conservative value compared to the -70 m bias and 600 m standard deviation found by Homeyer *et al.* [2010]) to mark the uncertainty of the GFS tropopause in quantifying the cloud top distribution.

[37] Figure 7 shows the seasonal maps of above the tropopause cloud top frequency, calculated in  $2^\circ \times 3^\circ$  latitude-longitude bins for cloud tops higher than 0.5 km above the tropopause, with the consideration of the uncertainty. The map terminates at  $\pm 75^\circ$  degrees latitude in order to focus on the tropics and midlatitudes but not the polar regions. The seasonal mean subtropical jet positions are also shown, using the 200 hPa horizontal wind speed of 30 and 40 m/s, which marks the transition between the tropics and the extratropics. The cloud top frequency is given in the range of 4–24%, which we found to highlight the region of significant occurrence and to include the highest frequency, with an exception of the western Pacific during DJF. In that

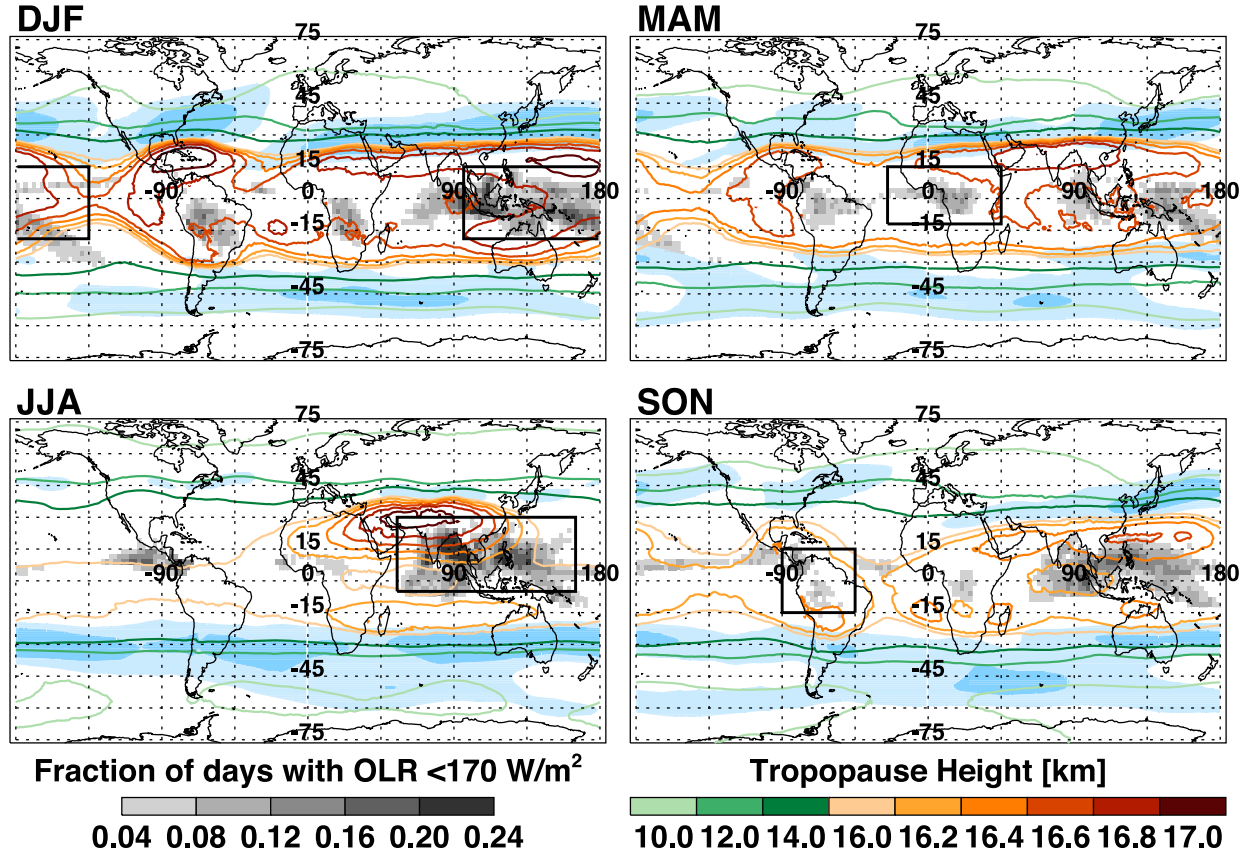


**Figure 8.** Seasonal mean tropopause height maps for the same time period as that shown in Figure 6. GFS/FNL data are used to compute the mean. Also shown is frequency of days with outgoing longwave radiation (OLR) under  $170 \text{ W/m}^2$  for the same period of time and the jet streams (30 and 40 m/s, blue shading).

region, there are a small fraction ( $\sim 2\%$ ) of bins that exceed 24%. The highest two bins (30% and 32%) are near northern Australia ( $14^\circ\text{--}16^\circ\text{S}$ ,  $126^\circ\text{--}129^\circ\text{E}$ ) and near the Solomon Islands ( $8^\circ\text{--}10^\circ\text{S}$ ,  $162^\circ\text{--}165^\circ\text{E}$ ).

[38] The seasonal geographical distributions of high-frequency regions in Figure 7 show a broad consistency with various previous studies of tropical cirrus cloud distributions [e.g., Nazaryan *et al.*, 2008; Sassen *et al.*, 2009;

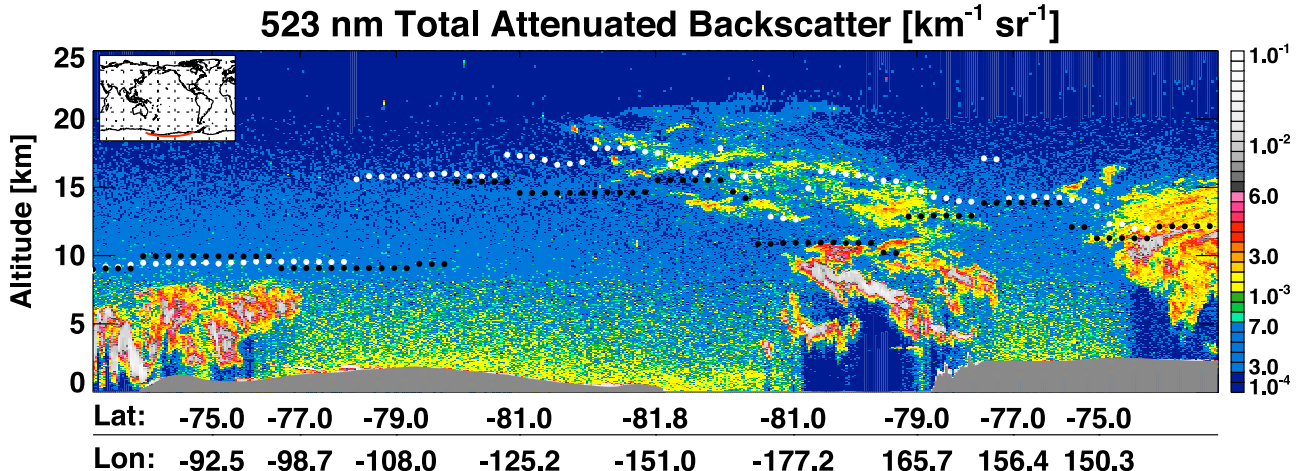


**Figure 9.** CALIPSO lidar 532 nm attenuated backscatter cross section over Antarctica on 1 August 2007 and the thermal tropopause from the models (white dots for the GFS tropopause and black dots for the GEOS5 tropopause included in the CALIPSO data file). The gray shaded areas indicate the elevation from a digital elevation model included in the CALIPSO files.

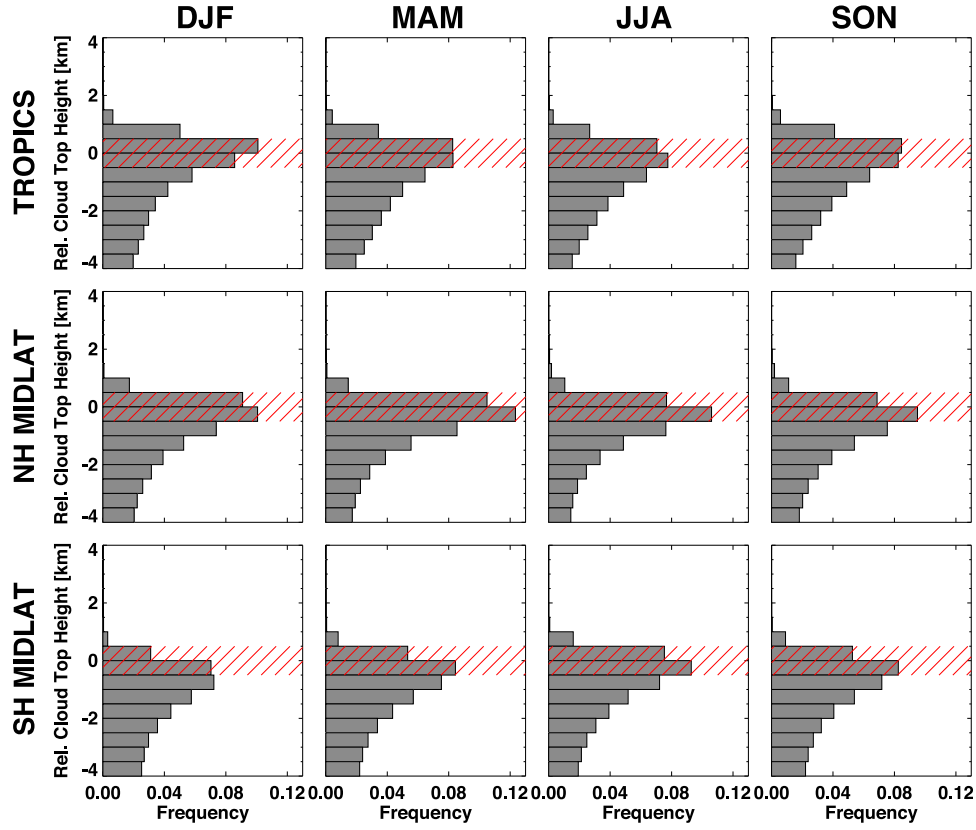


**Figure 10.** Zonal statistics of cloud top frequency of occurrence in the tropopause-relative coordinates for the tropics ( $20^{\circ}\text{S}$ – $20^{\circ}\text{N}$ ) and midlatitudes ( $40^{\circ}\text{N}$ – $60^{\circ}\text{N}$  and  $40^{\circ}\text{S}$ – $60^{\circ}\text{S}$ ) for four seasons. All 4 years of data are used. The GFS tropopause level is shown with  $\pm 0.5$  km uncertainty by the red stippling.

[39] As a companion graphic, we show the seasonal mean tropopause height for the same time period in Figure 8, which provides an altitude reference for the cloud top frequency in Figure 7. Also shown in Figure 8 are statistics of deep convection based on the frequency of OLR below  $170 \text{ W/m}^2$ . The OLR data is used here as a proxy for an independent measurement of deep convection. The OLR flux value of  $170 \text{ W/m}^2$  is estimated to be  $\sim 235^{\circ}\text{K}$  in brightness temperature and has been used in previous studies to select deep convective events [Massie *et al.*, 2002]. The frequency of occurrence for events shows a strong resemblance with the above the tropopause cloud top statistics in geographic distribution. Note that both data, although based on different

measurements, are from polar orbiting satellites with similar equator crossing times. Although not the focus of this study, it is interesting to note that the regions of high tropical tropopause (16.5 or higher) and their relationship with the low OLR distribution roughly follows the Gill solution [Gill, 1980], relating the equator centered heating and its off-equatorial response.

[40] Although our study focuses on the tropics and the midlatitudes, a brief discussion of the polar winter conditions is necessary here to explain the significant cloud top fractions in the winter polar region shown in Figure 7, especially near Antarctica during JJA. Quite different from the tropics, these distributions should be considered artifacts resulting from the anomalous temperature structure in the polar winter season [e.g., Highwood *et al.*, 2000]. Owing to the strong influence of the polar vortex, the temperature structure there often does not support a well-defined tropopause. The frequent presence of vertically extending polar stratospheric clouds is also part of the structure. Figure 9 shows an example highlighting the situation. Under these conditions, a tropopause-based analysis is not very meaningful.

[41] To characterize the vertical distribution and further quantify the above the tropopause cloud top occurrences, we present two sets of vertically binned statistics. The first set (Figure 10) includes global zonal statistics for the tropics ( $20^{\circ}\text{S}$ – $20^{\circ}\text{N}$ ), northern midlatitudes ( $40^{\circ}$ – $60^{\circ}\text{N}$ ) and southern midlatitudes ( $40^{\circ}$ – $60^{\circ}\text{S}$ ) and in all four seasons. The second set (Figure 11) includes four selected seasons and regions, as indicated by the rectangles in Figure 7, where

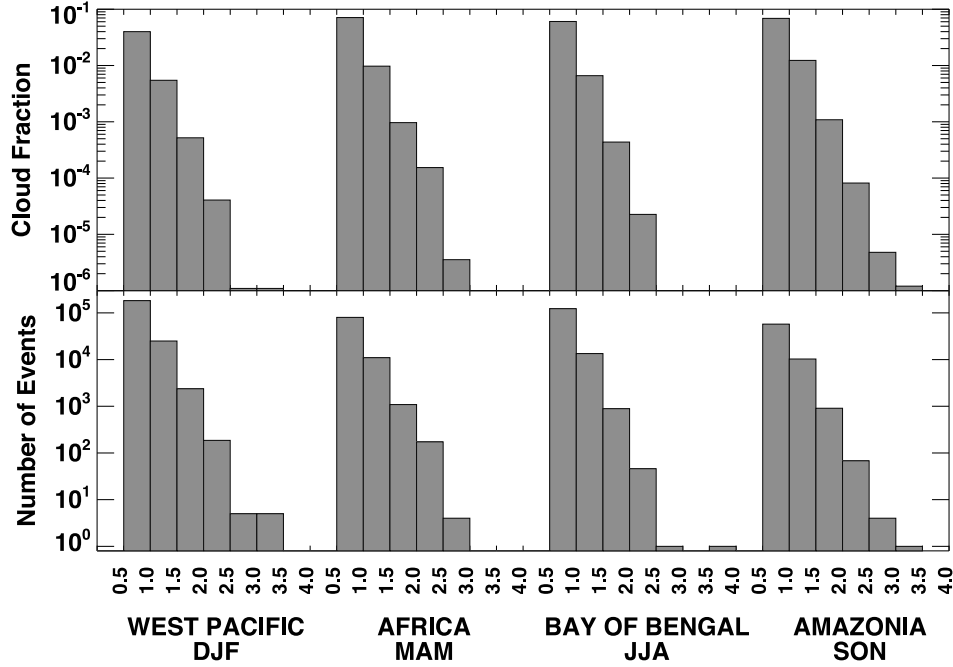


**Figure 11.** Above the tropopause cloud top distributions for the four selected regions and seasons as labeled. These regions are shown in the maps in Figures 7 and 8. The top histograms are regional fractions. The total numbers of overshooting events are given in the bottom histograms. Note all histograms are in log scales.

high occurrences of above the tropopause cloud tops are found. In both cases, the cloud tops are binned for every 0.5 km in altitude relative to the tropopause. The two sets complement each other, providing the quantitative information for the average behavior and the extreme regions.

[42] The most outstanding common feature in the zonal cloud top vertical structure in Figure 10 is the maximum occurrence near the tropopause. Here the tropopause level is given with an uncertainty of  $\pm 0.5$  km (shown by the red stippling). The only case the occurrence peaked arguably under the tropopause is the southern midlatitudes DJF group. These maxima range from  $\sim 8\%$  to  $\sim 10\%$  in the tropics,  $\sim 10\%$  to  $12\%$  in NH midlatitudes, and  $\sim 6\%$  to  $\sim 10\%$  in SH midlatitudes. Note that the highest fraction is in the NH midlatitudes during spring (MAM).

[43] Quantitatively, in the midlatitudes the zonal fraction 0.5 km or higher above the tropopause is less than 2% and largely in the vertical layer of 0.5–1.0 km above the tropopause. The layer 1.0–1.5 km above the tropopause has less than 0.1% except NH summer (JJA) and fall (SON) seasons, which have approximately 0.2% occurrences. We do not consider these fractions to be significant largely because we cannot rule out that this is not entirely due to the uncertainty of the tropopause height determination as indicated in Figure 3. In the tropics, the zonal fraction 1 km above the tropopause is less than 1%. These will be further examined in regional statistics.

[44] Four regions with significant above the tropopause cloud tops are selected for quantifying regional statistics. These are the western Pacific in the DJF season, central Africa in the MAM season, Asian monsoon/Bay of Bengal for the JJA season, and the Amazon for the SON season. The areas used in the calculation are marked on the Figures 7

and 8 maps (rectangles). For each of the regions, we calculated the regional fraction for each 0.5 km bin above the tropopause. We also counted the absolute number of events during the 4 year data period. These quantities are shown in a log scale for clarity (Figure 11).

[45] Figure 11 is not intended to compare the relative contributions of the regions but mostly to view the vertical distributions of the above the tropopause events. With that said, the four regions have strong similarities in decreasing fraction above 0.5 km relative to the tropopause, roughly 1 order of magnitude in each 0.5 km bin. Using Africa/MAM as an example, the fractions for 0.5–2 km above the LRT in 0.5 km steps are 7%, 0.9%, and 0.09%, respectively. The absolute number of events (given in Table 1) above 2.5 km relative to the tropopause is very small. The largest is 10 events (all four years) in the western Pacific, which includes the island chains where the conditions of vigorous deep convection exist. Note again that the sampling of CALIPSO does not allow a fair representation of the afternoon convection maximum over land.

## 7. Role of the Cold Point Tropopause: An Alternative Perspective of Overshooting

[46] The above the tropopause cloud top statistics discussed in section 6 are calculated in reference to the GFS lapse rate thermal tropopause. In the tropics, the cold point thermal tropopause should be physically more relevant to the cloud top. The difference between the LRT and CPT in the tropics has been a subject of a number of prior studies [e.g., Highwood and Hoskins, 1998; Seidel *et al.*, 2001] and is not the subject of this study. Here, we present a limited analysis using a small set of data to discuss a perspective

**Table 1.** Events as Shown in the Bottom Histograms of Figure 11

	Number of Events			
	December–February, Western Pacific	March–May, Africa	June–August, Bay of Bengal	September–November, Amazon
0.5–1 km	182,875	80,087	123,227	57,437
1–1.5 km	24,972	10,974	13,441	10,282
1.5–2 km	2,372	1,089	888	908
2–2.5 km	186	173	46	68
2.5–3 km	5	4	1	4
3–3.5 km	5	0	0	1
3.5–4 km	0	0	1	0

relating the temperature structure near the tropopause to the high occurrence of cloud tops above the LRT. The small set of temperature sounding profile data ( $\sim 200$  sondes) are from Alajuela, Costa Rica, obtained during the TC4 experiment period July to August 2007 [Pfister *et al.*, 2010; Selkirk *et al.*, 2010]. We derive both LRT and CPT for each profile, and the comparisons are shown in Figure 12.

[47] Consistent with previous studies, comparisons in Figure 12 show that although the LRT and CPT agree in many cases, the LRT is often below CPT. The difference can

often be up to 2.5 km. We further contrast the temperature structure for the group with good LRT/CPT agreement and a group where LRT/CPT differences are 2 km or greater. The two groups of temperature profiles are displayed in the cold point relative coordinates. The two groups of temperature profiles show very different characteristics in the UTLS region. The second group shows a much more significant wave structure below the cold point, associated with it are gradient changes  $\sim 2$  km below the cold point, which in turn appear to be responsible for the LRT and CPT separation.

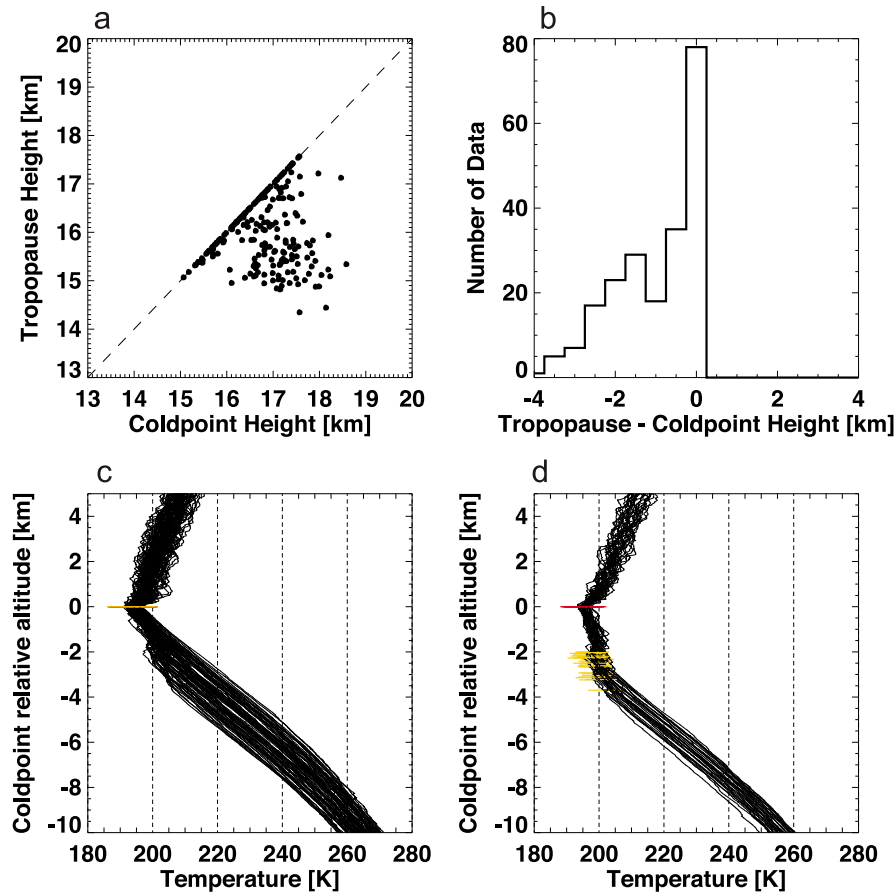


**Figure 12.** (a and b) Comparisons of the thermal tropopause and the cold-point tropopause, using high-resolution radiosonde data during the Tropical Chemistry, Cloud, and Climate Coupling (TC4) campaign (summer 2007). Approximately 200 profiles are used. (c and d) Two groups of temperature profiles displayed in altitude relative to the cold point. Figure 12c shows profiles that have good thermal-cold-point agreement (points along the 1 to 1 line in Figure 12a). Figure 12d shows the profiles with large thermal-cold-point separations (2 km or more apart). The red thin line (at the level 0) marks the cold-point level, and the yellow thin lines indicate the level of LRT for each profile.

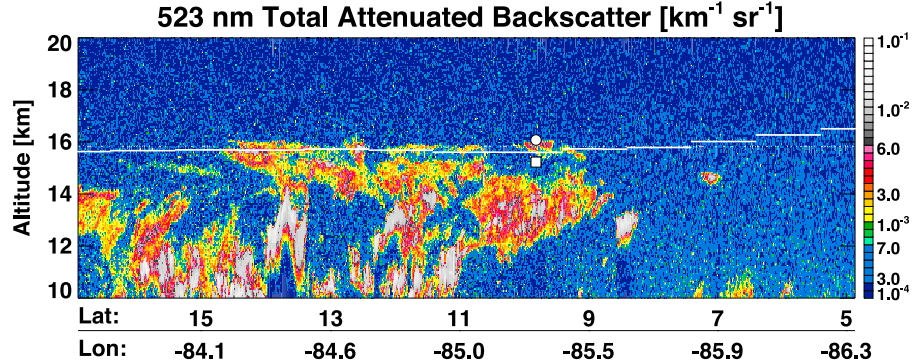


**Figure 13.** Colocated CALIPSO cross section and radiosonde profile from 3 July 2007. The thermal tropopause from GFS (white lines) and from the radiosonde temperature profile (white square) and the cold-point tropopause (white dot) from a sonde launched on 3 July 2007 at 0600 UTC from Alajuela, Costa Rica (latitude: 9.9°, longitude: -84.22°), are shown.

These gravity wave induced temperature anomalies are much better illustrated and discussed by Pfister *et al.* [2010] and Selkirk *et al.* [2010]. Here we mostly focus on the LRT and CPT separation. It is known that in the region of deep convection, the temperature in the UTLS region is strongly perturbed by waves of various types [e.g., Tsuda *et al.*, 1994; Holton *et al.*, 2001; Evan and Alexander, 2008; Fujiwara *et al.*, 2009; Pfister *et al.*, 2010]. The anomalous temperature structure may be an underlying factor of high occurrence of cloud tops above the LRT in the regions found in this study. In other words, a significant above the LRT fraction shown in section 6 may in fact be associated with the separation of the CPT and the LRT. Although they are above the LRT, they may still be below the CPT. When this is indeed the case, these clouds are likely in situ cirrus formed in response to the temperature perturbation, but not by convective overshooting. Alternatively, these clouds could be a result of convective detrainment above the LRT but below the CPT where the relative humidity is still high and the clouds can persist. These hypotheses need to be addressed in future studies.

[48] Figure 13 gives an example for this scenario using CALIPSO level-1 532 nm lidar cross section, GFS LRT, and a pair of LRT and CPT using a colocated sonde profile. In this case, the CPT and LRT are separated by ~1 km. A thin layer of cloud is seen to be above the GFS and the radiosonde LRT but is below the radiosonde CPT.

[49] Although we cannot conclude on the basis of this single example, we speculate that a significant amount of events above the LRT derived in section 6 is a result of the regions' large separation of LRT and CPT due to the wave activity. A systematic investigation using high-resolution data is required for a more conclusive study.

## 8. Conclusions and Discussions

[50] We have examined the cloud top distribution in relation to the tropopause using four years of CALIPSO data. This analysis is important for understanding the two-way interaction between the clouds and the thermal and dynamical structure of the UTLS. This analysis leads to a number of conclusions.

[51] The tropopause appears to be a significant boundary in the structure of the global cloud top distribution. This is

especially evident in the zonal vertical cloud top statistics where the peak frequency of the highest cloud top is centered at the thermal tropopause both in the tropics and the extratropics (Figure 10).

[52] With the consideration of the tropopause height uncertainty, we cannot conclude significant occurrence of cloud tops above the LRT outside the tropics, with the exception of the polar winter season, where the temperature structure often does not support a well-defined tropopause and polar stratospheric clouds form frequently. Analyses of cloud top relative to the tropopause under these conditions are not meaningful. Our analyses show that there is under 2% cloud top at 0.5 km above the GFS tropopause in NH midlatitude in zonal average. This is a significantly different conclusion from that in Dessler's [2009] work, in which up to 40% above the tropopause occurrence was found in NH midlatitudes. We speculate that this is due to the uncertainty of the tropopause product used.

[53] In the tropics, there are regions of high-frequency cloud top occurrences above the LRT. These regions and seasons are known for conditions of active convection on the basis of previous analyses and observations [Liu *et al.*, 2007; Yang *et al.*, 2010]. Although these events are small fractions in the zonal average sense (5% or less), they are very significant regionally (up to 24%).

[54] In these high-frequency regions, the cloud tops are largely limited to 2.5 km above the LRT tropopause vertically. The separation of the CPT and LRT may be a significant factor for these apparent over the tropopause events. The observed above the tropopause cloud tops may not necessarily be convective overshooting, and may at least in part be associated with severe perturbations of the temperature structure in the tropopause region due to the various waves excited by the convection. This is an alternative interpretation based on a small number of radiosonde profiles and isolated cases. More conclusive analyses will require further studies.

[55] Note that the results shown in this paper are based on CALIPSO level-2 CLAY data, which contain features with the base of the layer below the tropopause. The layers with both base and top above the tropopause are excluded from the CLAY data but included in the aerosol layer (ALAY) data. Although classifying clouds and aerosol is beyond the scope of this work, we estimated the potential impact of the

exclusion using the ALAY data for the 2007 JJA season. The results show that if all features in the ALAY data are actually clouds, the fraction of cloud top above the tropopause (excluding the polar region) as shown in Figure 7 will increase for about 1% but there will be no qualitative change in the conclusion.

[56] The analyses we have done do not lead to understanding of what type of clouds, convective detrainment or in situ cirrus, are contributing to the events at or above the tropopause. Although the significant presence are over the convectively active regions, the analysis shown in section 7 argues that both overshooting convection and wave perturbation induced CPT-LRT separation can contribute to the above the LRT fractions shown in this study.

[57] The result of this analysis is specifically afforded by CALIPSO capabilities and limitations. We note here two specific limitations. The first one is related to the sampling time. The 0130 and 1330 local equator crossing time of CALIPSO satellite will not allow an adequate sampling of afternoon convection, which is active over land. Some of the most vigorous convection events are therefore not included in this analysis. The second limitation is related to the CALIPSO detection limits of optical depth greater than 0.01. The instrument is found to miss the very thin cirrus, like those measured by airborne cloud lidar during the TC4 experiment with optical depth between  $10^{-4}$  and  $10^{-3}$ . Analyses show that this may produce a significant underestimate of cirrus near the tropopause [Davis *et al.*, 2010].

[58] Our study also shows that using the tropopause relative coordinates and accurate tropopause determination are important for this type of analyses. An important factor that leads to significant differences in conclusions between this study and that of Dessler [2009] is likely the tropopause uncertainty and comparing the cloud tops with the average tropopause height.

[59] With increasing availability of high-resolution soundings from both the ground-based sondes and space based GPS data, further investigations using higher-resolution temperature data is a possible next step. Combined analyses of cloud top and cloud properties are also necessary to shed light on the type of clouds and to improve our understanding of the mechanisms controlling the high clouds. These will be pursued in a future study.

[60] **Acknowledgments.** The National Center for Atmospheric Research is sponsored by the National Science Foundation. The authors thank Steve Massie and Eric Jensen for helpful discussions. CALIPSO data were obtained from the NASA Langley Research Center Atmospheric Science Data Center.

## References

- Bethan, S., G. Vaughan, and S. J. Reid (1996), A comparison of ozone and thermal tropopause heights and the impact of tropopause definition on quantifying the ozone content of the troposphere, *Q. J. R. Meteorol. Soc.*, **122**, 929–944, doi:10.1002/qj.49712253207.
- Birner, T. (2006), Fine-scale structure of the extratropical tropopause region, *J. Geophys. Res.*, **111**, D04104, doi:10.1029/2005JD006301.
- Bony, S., W. D. Collins, and D. W. Fillmore (2000), Indian ocean low clouds during the winter monsoon, *J. Clim.*, **13**, 2028–2043, doi:10.1175/1520-0442(2000)013<2028:IOLCDT>2.0.CO;2.
- Corti, T., B. P. Luo, Q. Fu, H. Vömel, and T. Peter (2006), The impact of cirrus clouds on tropical troposphere to stratosphere transport, *Atmos. Chem. Phys.*, **6**, 2539–2547, doi:10.5194/acp-6-2539-2006.
- Corti, T., et al. (2008), Unprecedented evidence for deep convection hydrating the tropical stratosphere, *Geophys. Res. Lett.*, **35**, L10810, doi:10.1029/2008GL033641.
- Danielsen, E. F. (1993), In situ evidence of rapid, vertical, irreversible transport of lower tropospheric air into the lower tropical stratosphere by convective cloud turrets and by larger-scale upwelling in tropical cyclones, *J. Geophys. Res.*, **98**, 8665–8681, doi:10.1029/92JD02954.
- Davis, S., et al. (2010), In situ and lidar observations of tropopause subvisible cirrus clouds during TC4, *J. Geophys. Res.*, **115**, D00J17, doi:10.1029/2009JD013093.
- Dessler, A. E. (2009), Clouds and water vapor in the Northern Hemisphere summertime stratosphere, *J. Geophys. Res.*, **114**, D00H09, doi:10.1029/2009JD012075.
- Dessler, A. E., S. P. Palm, W. D. Hart, and J. D. Spinhirne (2006), Tropopause-level thin cirrus coverage revealed by ICESat/Geoscience Laser Altimeter System, *J. Geophys. Res.*, **111**, D08203, doi:10.1029/2005JD006586.
- Dethof, A., A. O'Neill, J. M. Slingo, and H. G. J. Smit (1999), A mechanism for moistening the lower stratosphere involving the Asian summer monsoon, *Q. J. R. Meteorol. Soc.*, **125**, 1079–1106.
- Devasthale, A., and S. Fueglistaler (2010), A climatological perspective of deep convection penetrating the TTL during the Indian summer monsoon from the AVHRR and MODIS instruments, *Atmos. Chem. Phys.*, **10**, 4573–4582, doi:10.5194/acp-10-4573-2010.
- Evan, S., and M. J. Alexander (2008), Intermediate-scale tropical inertia gravity waves observed during the TWP-ICE campaign, *J. Geophys. Res.*, **113**, D14104, doi:10.1029/2007JD009289.
- Fu, R., et al. (2006), Short circuit of water vapor and polluted air to the global stratosphere by convective transport over the Tibetan Plateau, *Proc. Natl. Acad. Sci. U. S. A.*, **103**, 5664–5669, doi:10.1073/pnas.0601584103.
- Fujiwara, M., et al. (2009), Cirrus observations in the tropical tropopause layer over the western Pacific, *J. Geophys. Res.*, **114**, D09304, doi:10.1029/2008JD011040.
- Gill, A. E. (1980), Some simple solutions for heat-induced tropical circulation, *Q. J. R. Meteorol. Soc.*, **106**, 447–462, doi:10.1002/qj.49710644905.
- Haladay, T., and G. Stephens (2009), Characteristics of tropical thin cirrus clouds deduced from joint CloudSat and CALIPSO observations, *J. Geophys. Res.*, **114**, D00A25, doi:10.1029/2008JD010675.
- Hanisco, T. F., et al. (2007), Observations of deep convective influence on stratospheric water vapor and its isotopic composition, *Geophys. Res. Lett.*, **34**, L04814, doi:10.1029/2006GL027899.
- Hartmann, D. L., J. R. Holton, and Q. Fu (2001), The heat balance of the tropical tropopause, cirrus, and stratospheric dehydration, *Geophys. Res. Lett.*, **28**, 1969–1972, doi:10.1029/2000GL012833.
- Heymann, A. J. (1986), Ice particles observed in a cirriform cloud at  $-83^{\circ}\text{C}$  and implications for polar stratospheric clouds, *J. Atmos. Sci.*, **43**, 851–855, doi:10.1175/1520-0469(1986)043<0851:IPOIAC>2.0.CO;2.
- Highwood, E. J., and B. J. Hoskins (1998), The tropical tropopause, *Q. J. R. Meteorol. Soc.*, **124**, 1579–1604, doi:10.1002/qj.49712454911.
- Highwood, E. J., B. J. Hoskins, and P. Berrisford (2000), Properties of the Arctic tropopause, *Q. J. R. Meteorol. Soc.*, **126**, 1515–1532, doi:10.1256/smscj.56514.
- Hoerling, M. P., T. D. Schaack, and A. J. Lenzen (1991), Global objective tropopause analysis, *Mon. Weather Rev.*, **119**, 1816–1831, doi:10.1175/1520-0493(1991)119<1816:GOTA>2.0.CO;2.
- Hoinka, K. P. (1997), The tropopause: Discovery, definition and demarcation, *Meteorol. Z.*, **6**, 281–303.
- Holton, J. R., and A. Gettelman (2001), Horizontal transport and the dehydration of the stratosphere, *Geophys. Res. Lett.*, **28**, 2799–2802, doi:10.1029/2001GL013148.
- Holton, J. R., P. H. Haynes, A. R. Douglass, R. B. Rood, and L. Pfister (1995), Stratosphere-troposphere exchange, *Rev. Geophys.*, **33**, 403–439, doi:10.1029/95RG02097.
- Holton, J. R., M. J. Alexander, and M. T. Boehm (2001), Evidence for short vertical wavelength Kelvin waves in the Department of Energy-Atmospheric Radiation Measurement Nauru99 radiosonde data, *J. Geophys. Res.*, **106**, 20125–20,129.
- Homeyer, C. R., K. P. Bowman, and L. L. Pan (2010), Extratropical tropopause transition layer characteristics from high-resolution sounding data, *J. Geophys. Res.*, **115**, D13108, doi:10.1029/2009JD013664.
- Hoskins, B. J. (1991), Towards a PV- $\Theta$  view of the general circulation, *Tellus, Ser. A*, **43**, 27–35.
- James, R., M. Bonazzola, B. Legras, K. Surbled, and S. Fueglistaler (2008), Water vapor transport and dehydration above convective outflow during Asian monsoon, *Geophys. Res. Lett.*, **35**, L20810, doi:10.1029/2008GL035441.
- Jensen, E. J., A. S. Ackerman, and J. A. Smith (2007), Can overshooting convection dehydrate the tropical tropopause layer?, *J. Geophys. Res.*, **112**, D11209, doi:10.1029/2006JD007943.

- Khaykin, S., J.-P. Pommereau, L. Korshunov, V. Yushkov, J. Nielsen, N. Larsen, T. Christensen, A. Garnier, A. Lukyanov, and E. Williams (2009), Hydration of the lower stratosphere by ice crystal geysers over land convective systems, *Atmos. Chem. Phys.*, **9**, 2275–2287, doi:10.5194/acp-9-2275-2009.
- Kunz, A., P. Konopka, R. Mueller, and L. L. Pan (2011), The dynamical tropopause based on isentropic PV gradient, *J. Geophys. Res.*, **116**, D01110, doi:10.1029/2010JD014343.
- Liebmann, B., and C. A. Smith (1996), Description of a complete (interpolated) outgoing longwave radiation dataset, *Bull. Am. Meteorol. Soc.*, **77**, 1275–1277.
- Liu, C., and E. J. Zipser (2005), Global distribution of convection penetrating the tropical tropopause, *J. Geophys. Res.*, **110**, D23104, doi:10.1029/2005JD006063.
- Liu, C., and E. J. Zipser (2009), Implications of the day versus night differences of water vapor, carbon monoxide, and thin cloud observations near the tropical tropopause, *J. Geophys. Res.*, **114**, D09303, doi:10.1029/2008JD011524.
- Liu, C., E. Zipser, and S. W. Nesbitt (2007), Global distribution of tropical deep convection: Different perspectives using infrared and radar as the primary data source, *J. Clim.*, **20**, 489–503, doi:10.1175/JCLI4023.1.
- Liu, C., E. J. Zipser, G. G. Mace, and S. Benson (2008), Implications of the differences between daytime and nighttime CloudSat observations over the tropics, *J. Geophys. Res.*, **113**, D00A04, doi:10.1029/2008JD009783.
- Massie, S., A. Gettelman, W. Randel, and D. Baumgardner (2002), Distribution of tropical cirrus in relation to convection, *J. Geophys. Res.*, **107**(D21), 4591, doi:10.1029/2001JD001293.
- Massie, S. T., J. Gille, C. Craig, R. Khosravi, J. Barnett, W. Read, and D. Winker (2010), HIRDLS and CALIPSO observations of tropical cirrus, *J. Geophys. Res.*, **115**, D00H11, doi:10.1029/2009JD012100.
- Nazaryan, H., M. P. McCormick, and W. P. Menzel (2008), Global characterization of cirrus clouds using CALIPSO data, *J. Geophys. Res.*, **113**, D16211, doi:10.1029/2007JD009481.
- Nee, J. B., C. N. Len, W. N. Chen, and C. I. Lin (1998), Lidar observation of the cirrus cloud in the tropopause at Chung-Li (25°N, 121°E), *J. Atmos. Sci.*, **55**, 2249–2257, doi:10.1175/1520-0469(1998)055<2249:LOOTCC>2.0.CO;2.
- Newell, R. E., and S. Gould-Stewart (1981), A stratospheric fountain?, *J. Atmos. Sci.*, **38**, 2789–2796, doi:10.1175/1520-0469(1981)038<2789:ASF>2.0.CO;2.
- Noël, V., and M. Haeffelin (2007), Midlatitude cirrus clouds and multiple tropauses from a 2002–2006 climatology over the SIRTA observatory, *J. Geophys. Res.*, **112**, D13206, doi:10.1029/2006JD007753.
- Pan, L. L., E. J. Hintsa, E. M. Stone, E. M. Weinstock, and W. J. Randel (2000), The seasonal cycle of water vapor and saturation vapor mixing ratio in the extratropical lowermost stratosphere, *J. Geophys. Res.*, **105**, 26,519–26,530, doi:10.1029/2000JD900401.
- Pan, L. L., W. J. Randel, B. L. Gary, J. M. Mahoney, and E. J. Hintsa (2004), Definitions and sharpness of the extratropical tropopause: A trace gas perspective, *J. Geophys. Res.*, **109**, D23103, doi:10.1029/2004JD004982.
- Pan, L. L., et al. (2007), Chemical behavior of the tropopause observed during the Stratosphere-Troposphere Analyses of Regional Transport experiment, *J. Geophys. Res.*, **112**, D18110, doi:10.1029/2007JD008645.
- Pan, L. L., W. J. Randel, J. C. Gille, W. D. Hall, B. Nardi, S. Massie, V. Yudin, R. Khosravi, P. Konopka, and D. Tarasick (2009), Tropospheric intrusions associated with the secondary tropopause, *J. Geophys. Res.*, **114**, D10302, doi:10.1029/2008JD011374.
- Pan, L. L., et al. (2010), The Stratosphere-Troposphere Analyses of Regional Transport 2008 experiment, *Bull. Am. Meteorol. Soc.*, **91**, 327–342, doi:10.1175/2009BAMS2865.1.
- Park, M., W. J. Randel, L. K. Emmons, and N. J. Livesey (2009), Transport pathways of carbon monoxide in the Asian summer monsoon diagnosed from Model of Ozone and Related Tracers (MOZART), *J. Geophys. Res.*, **114**, D08303, doi:10.1029/2008JD010621.
- Pfister, L., H. B. Selkirk, D. O. Starr, K. Rosenlof, and P. A. Newman (2010), A meteorological overview of the TC4 mission, *J. Geophys. Res.*, **115**, D00J12, doi:10.1029/2009JD013316.
- Posselt, D. J., G. L. Stephens, and M. Miller (2008), CLOUDSAT: Adding a new dimension to a classical view of extratropical cyclones, *Bull. Am. Meteorol. Soc.*, **89**, 599–609, doi:10.1175/BAMS-89-5-599.
- Randel, W. J., and M. Park (2006), Deep convective influence on the Asian summer monsoon anticyclone and associated tracer variability observed with Atmospheric Infrared Sounder (AIRS), *J. Geophys. Res.*, **111**, D12314, doi:10.1029/2005JD006490.
- Randel, W. J., F. Wu, A. Gettelman, J. M. Russell III, J. M. Zawodny, and S. J. Oltmans (2001), Seasonal variation of water vapor in the lower strato-
- sphere observed in Halogen Occultation Experiment data, *J. Geophys. Res.*, **106**, 14,313–14,325, doi:10.1029/2001JD900048.
- Randel, W. J., M. Park, L. Emmons, D. Kinnison, P. Bernath, K. A. Walker, C. Boone, and H. Pumphrey (2010), Asian monsoon transport of pollution to the stratosphere, *Science*, **328**, 611–613, doi:10.1126/science.1182274.
- Rienecker, M. (2008), File specification for GEOS-5 DAS gridded output, *NASA Tech. Rep.*, *GMAO-1001v6.4*, 54 pp.
- Rosenfield, J. E., D. B. Considine, M. R. Schoeberl, and E. V. Browell (1998), The impact of subvisible cirrus clouds near the tropical tropopause on stratospheric water vapor, *Geophys. Res. Lett.*, **25**, 1883–1886, doi:10.1029/98GL01294.
- Sassen, K., Z. Wang, and D. Liu (2009), Cirrus clouds and deep convection in the tropics: Insights from CALIPSO and CloudSat, *J. Geophys. Res.*, **114**, D00H06, doi:10.1029/2009JD011916.
- Seidel, D. J., and W. J. Randel (2007), Recent widening of the tropical belt: Evidence from tropopause observations, *J. Geophys. Res.*, **112**, D20113, doi:10.1029/2007JD008861.
- Seidel, D. J., R. J. Ross, J. K. Angell, and G. C. Reid (2001), Climatological characteristics of the tropical tropopause as revealed by radiosondes, *J. Geophys. Res.*, **106**, 7857–7878, doi:10.1029/2000JD900837.
- Selkirk, H. B. (1993), The tropopause cold trap in the Australian monsoon during STEP/AMEX 1987, *J. Geophys. Res.*, **98**, 8591–8610, doi:10.1029/92JD02932.
- Selkirk, H. B., H. Vömel, J. M. Valverde Canossa, L. Pfister, J. A. Diaz, W. Fernández, J. Amador, W. Stoltz, and G. S. Peng (2010), Detailed structure of the tropical upper troposphere and lower stratosphere as revealed by balloon sonde observations of water vapor, ozone, temperature, and winds during the NASA TCSP and TC4 campaigns, *J. Geophys. Res.*, **115**, D00J19, doi:10.1029/2009JD013209.
- Shapiro, M. A. (1980), Turbulent mixing within tropopause folds as a mechanism for the exchange of chemical constituents between the stratosphere and troposphere, *J. Atmos. Sci.*, **37**, 994–1004, doi:10.1175/1520-0469(1980)037<0994:TMWTF>2.0.CO;2.
- Sherwood, S. C., and A. E. Dessler (2001), A model for transport across the tropical tropopause, *J. Atmos. Sci.*, **58**, 765–779, doi:10.1175/1520-0469(2001)058<0765:AMFTAT>2.0.CO;2.
- Smith, J. B., E. J. Hintsa, N. T. Allen, R. M. Stimpfle, and J. G. Anderson (2001), Mechanisms for midlatitude ozone loss: Heterogeneous chemistry in the lowermost stratosphere?, *J. Geophys. Res.*, **106**, 1297–1309, doi:10.1029/2000JD900464.
- Stephens, G. L., et al. (2002), The CloudSat mission and the A-train, *Bull. Am. Meteorol. Soc.*, **83**, 1771–1790, doi:10.1175/BAMS-83-12-1771.
- Suarez, M. J., et al. (2008), The GEOS-5 data assimilation system documentation of versions 5.0.1, 5.1.0, and 5.2.0, *NASA Tech. Rep.*, *TM-2008-104606*, vol. 27, 97 pp.
- Tilmes, S., et al. (2010), An aircraft-based upper troposphere lower stratosphere O<sub>3</sub>, CO, and H<sub>2</sub>O climatology for the Northern Hemisphere, *J. Geophys. Res.*, **115**, D14303, doi:10.1029/2009JD012731.
- Tsuda, T., Y. Murayama, H. Wirayosumarto, S. W. B. Harijono, and S. Kato (1994), Radiosonde observations of equatorial atmosphere dynamics over Indonesia: 1. Equatorial waves and diurnal tides, *J. Geophys. Res.*, **99**, 10,507–10,516, doi:10.1029/94JD00354.
- Tuck, A. F., et al. (1997), The Brewer-Dobson circulation in the light of high-altitude in situ aircraft observations, *Q. J. R. Meteorol. Soc.*, **123**, 1–69.
- Vaughan, M., K. A. Powell, R. E. Kuehn, S. A. Young, D. M. Winker, C. A. Hostetler, W. H. Hunt, Z. Liu, M. J. McGill, and B. J. Getzewich (2009), Fully automated detection of cloud and aerosol layers in the CALIPSO lidar measurements, *J. Atmos. Oceanic Technol.*, **26**, 2034–2050, doi:10.1175/2009TECHA1228.1.
- Winker, D. M., W. H. Hunt, and M. J. McGill (2007), Initial performance assessment of CALIOP, *Geophys. Res. Lett.*, **34**, L19803, doi:10.1029/2007GL030135.
- Winker, D. M., et al. (2010), The CALIPSO mission: A global 3D view of aerosols and clouds, *Bull. Am. Meteorol. Soc.*, **91**, 1211–1229, doi:10.1175/2010BAMS3009.1.
- World Meteorological Organization (WMO) (1957), Meteorology-a three-dimensional science: Second session for the commission for aerology, *WMO Bull.*, **6**, 134–138.
- Yang, Q., Q. Fu, and Y. Hu (2010), Radiative impacts of clouds in the tropical tropopause layer, *J. Geophys. Res.*, **115**, D00H12, doi:10.1029/2009JD012393.

L. A. Munchak and L. L. Pan, National Center for Atmospheric Research, 1850 Table Mesa Dr., PO Box 3000, Boulder, CO 80305, USA. (liwen@ucar.edu)